SCIENTIFIC REPORTS

OPEN

Pinned domain wall oscillator as a tuneable direct current spin wave emitter

Michele Voto, Luis Lopez-Diaz & Eduardo Martinez

Local perturbations in the relative orientation of the magnetic moments in a continuous magnetic system can propagate in the form of waves. These so-called spin waves represent a promising candidate as an information carrier for spin-based low-power applications. A localized, energy-efficient excitation of coherent and short-wavelength spin waves is a crucial technological requirement, and alternatives to excitation via the Oersted field of an alternating current must be explored. Here, we show how a domain wall pinned at a geometrical constriction in a perpendicularly magnetized thin nanowire emits spin waves when forced to rotate by the application of a low direct current flowing along the wire. Spin waves are excited by the in-plane stray field of the rotating domain wall and propagate at an odd harmonic of the domain wall rotation frequency in the direction of the electron's flow. The application of an external field, opposing domain wall depinning induced by the current, breaks the symmetry for spin wave propagation in the two domains, allowing emission in both directions but at different frequencies. The results presented define a new approach to manufacture tuneable high-frequency spin wave emitters of easy fabrication and low power consumption.

A spin wave (SW) is a propagating perturbation in the spin texture of a magnetic material in the form of a phase-coherent precession of the magnetic moments[1–3]. The quanta of spin waves are called magnons and the field investigating the transmission and processing of information mediated by spin waves is termed magnonics. Magnonics offers a promising new route for computing technology because it may overcome the limitations of complementary metal oxide semiconductor (CMOS) technology in terms of scalability and power consumption via a particle-less transmission of information[4–9] and by introducing new degrees of freedom encoded in spin waves' transport of angular momentum. Spin waves have short wavelengths at the technologically relevant GHz - low THz frequencies, allowing for integration with microwave electronics at the nanoscale[2]. The classical technique used to excite spin waves is via the Oersted field induced around a wire placed on top of the spin waves conduct from an ac current flowing through it[6,8,10]. This approach allows control of the frequency and wavelength of injected magnons, with the main drawback that the antenna width sets a lower bound for wavelength and limits the scalability of the device. An alternative way of inducing linear excitation of short-wavelength spin waves is through the uniform microwave excitation of a inhomogeneous magnetization texture[11,12]. The conversion of electron-carried angular momentum into magnons[13–15] and vice versa[10,16] allows for the exploitation of spintronics phenomena for the generation and detection of spin waves at the nanoscale and the embedding of magnonic circuitry in electronic-based devices. This novel field is called magnon-spintronics. Here, spin wave generation can be achieved by various localized excitations, such as electric field control of the magnetostrictive properties of materials[17–19] and spin transfer torque[20–22] (STT), generated either by a spin-polarized current flowing through a nanocontact[13,14] or via the spin current originated by the flow of charge current through an adjacent non-magnetic metal with large spin-orbit coupling[15,23–25].

It is known that a domain wall (DW) can emit spin waves during its motion[26–30] or under microwave linear excitation[12]; the use of an oscillating domain wall as a tuneable spin wave emitter excited by an alternate current, has been proposed by Van de Wiele and colleagues[31]. In their work, a strong pinning of the DW is achieved via ferromagnetic-ferroelectric coupling, and an ac current is used to generate DW oscillations that excite propagation of SWs in adjacent domains at an angle of 45° with respect to the magnetization orientation. The use of a DW permits SW excitation at wavelengths much shorter than can be achieved with common antennas and the change in ac frequency can, to some extent, regulate the emitted frequency. However,

Departamento de Física Aplicada, Universidad de Salamanca, Plaza de la Merced s/n, 37008, Salamanca, Spain. Correspondence and requests for materials should be addressed to M.V. (email: michele.voto@usal.es)
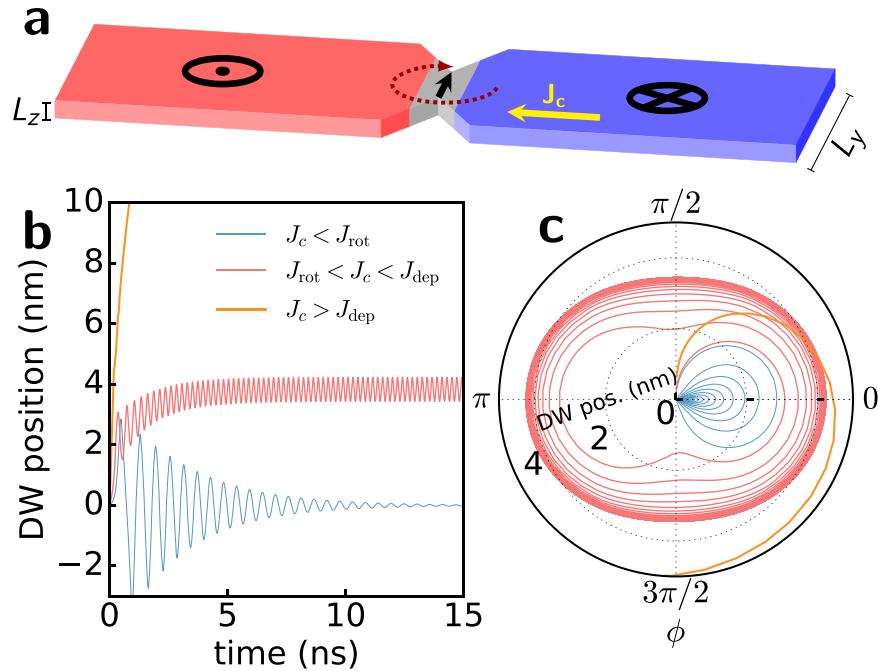
1

Figure 1. Scheme of the system under study and DW dynamics representation. (**a**) A DW located at a symmetric notch separates the up (red) and down (blue) domains. Current flows from right to left so that the induced rotation of the DW is clockwise. The in-plane direction of rotation is marked. (**b**) DW position as a function of time in micromagnetic simulations with current values below (dark blue line), inside (purple line) and above (orange line) the pinned rotation window. (**c**) Data from the same simulations as in (**b**) plotted to represent DW position q as the radial coordinate and the DW angle ϕ as the polar coordinate.

the realization of such a device presents some limitations: high current densities are required, the fabrication of hybrid ferromagnetic-ferroelectric structures is difficult, and the propagation of SWs in the 45° magnetized domains is non-trivial.

It was shown both analytically and numerically[32–35] that a DW pinned at a constriction in a perpendicularly magnetized nanowire could be led to self-sustained full in-plane rotation by the STT exerted on it by the injection of a low in-plane dc current while remaining pinned at a localized pinning site, thus creating a DW-based oscillator with frequencies in the GHz range, tuneable via the applied current intensity.

In this work we reconsider the DW oscillator set-up, schematically represented in Fig. 1a, and investigate, using micromagnetic simulations, the emission of SWs generated by such localized magnetization precession in a nanowire. By selecting an adequate wire width and constriction geometry, we can achieve a wide operating window in which we observe DW rotation at a current-dependent frequency (f_{DW}) that leads to unidirectional emission of SWs in the direction of electrons' flow at odd harmonics of f_{DW}. Because the SW frequency is a multiple of f_{DW}, the frequency of the emitted SWs can also be tuned by changing current intensity. Moreover, through the application of an external field opposing the force exerted on the DW by the current, the device operating window is extended and, at the same time, the symmetric dispersion relation for SWs in the two antiparallel domains is naturally split, which allows us to selectively propagate different harmonics along each domain. We identify the DW's in-plane stray field as the main factor responsible for SW excitation, whereas the unidirectionality is due to the asymmetric position of the DW below the geometrical constriction. This new concept of SW emitter has the attractive features of high coherence, a tuneable frequency up to tens of GHz and low power consumption (typical current of a few μA) by simply exploiting the stray field induced by geometrical patterning.

Results

We consider a DW trapped at a symmetric constriction in a narrow wire and a dc current flowing through it, as shown in Fig. 1a. The constriction acts as a pinning site for the DW and therefore, a minimum threshold current J_{dep} is required to depin the DW and propagate it through the nanowire. For current densities below this threshold, the DW remains pinned at a position where the restoring pinning force balances the driving STT force that pushes the DW away from the notch. However, a zero net driving force does not imply balance of the in-plane torques acting on the DW. In particular, if a current density is above a certain value J_{rot}, the in-plane component of the STT overcomes the shape anisotropy field torque[36], leading to sustained full in-plane rotation of the spins inside the DW[33,34]. Such a situation requires the fulfilment of precise conditions that we synthetically present below using a typical one-dimensional model[37–39] (see Methods), which provides a good approximation to complex DW dynamics in narrow wires. Within this model, the system is described using the position of the DW (q) with respect to its equilibrium position centred at the constriction and the in-plane orientation (ϕ) of the spins in the DW as the only degrees of freedom. The pinning caused by the constriction is modelled as a parabolic
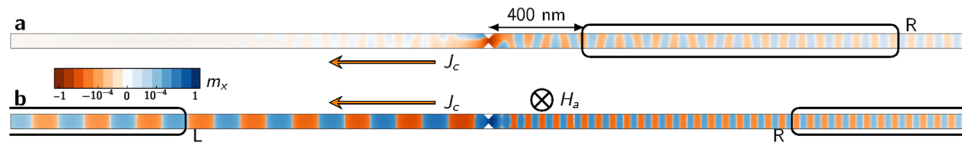
Figure 2. Snapshot of the magnetization dynamics representing the $m_x = M_x/M_s$ value. (**a**) A current density of $6.5 \times 10^{10}\,\mathrm{A\,m^{-2}}$ is injected. The region R on the right where m_x is sampled is enclosed by a rectangle. Unidirectional SW propagation towards the right can be observed. (**b**) Snapshot of the magnetization dynamics under the concurrent action of an in-plane current of $24 \times 10^{10}\,\mathrm{A\,m^{-2}}$ and an external field of 300 mT directed inside the plane to oppose DW depinning. A wire twice as long as in (**a**) is considered. Emission of SWs is observed both towards the right and the left at different frequencies and wavelengths; the sampled regions on the left (L) and right (R) are enclosed by black rectangles, and they extend for $2\,\mu$m.

potential well[34], which gives rise to a spring-like restoring field $H_p(q)$. Within this framework, pinned DW rotation is attained for current density values J_c in the range

$$J_{\mathrm{rot}} = \frac{eM_s}{P\mu_B}\frac{\gamma_0 \Delta H_K}{2} < J_c < \frac{eM_s}{P\mu_B}\frac{\alpha\gamma_0 \Delta H_p^{max}}{1+\alpha\beta} = J_{\mathrm{dep}}, \tag{1}$$

where e is the negative electron charge, M_s is the saturation magnetization, P the current polarization, μ_B is Bohr magneton, $\gamma_0 = 2.21 \times 10^5\,\mathrm{rad\,m\,A^{-1}s^{-1}}$ is the gyromagnetic ratio, Δ the domain wall width parameter, H_K the in-plane shape anisotropy field, H^{max}_p the maximum pinning field, α is Gilbert's damping parameter and β the degree of non-adiabaticity. The analytical derivation of such conditions can be found in section A of the supplementary information.

Data from micromagnetic simulations realized for three different cases, $J_{c,1} < J_{\mathrm{rot}} < J_{c,2} < J_{\mathrm{dep}} < J_{c,3}$ are shown in Fig. 1b, where the DW position is plotted as a function of time, and in Fig. 1c, where the position and in-plane DW angle are shown in polar coordinates. As can be observed, the DW reaches an equilibrium position for $J_c < J_{\mathrm{rot}}$ after a few nanoseconds, whereas for $J_c > J_{\mathrm{dep}}$, the DW rapidly depins from the notch. For $J_{\mathrm{rot}} < J_c < J_{\mathrm{dep}}$, however, the DW moves a few nanometres towards the right and slightly oscillates back and forth around this position while rotating in-plane.

To obtain a large operating window of the device, we tune the wire width and notch shape to obtain a low threshold current for the DW pinned rotation J_{rot} and a high threshold current for DW depinning J_{dep}. Because the $|\mathbf{J}_c|$ value is not constant in space and increases at the constriction, throughout the paper, we refer to its value as the nominal one away from the geometrical constriction. We select a wire width L_y of 60 nm, a thickness $L_z = 1$ nm and a notch depth of 20 nm, which gives us $J_{\mathrm{rot}} = 10^{10}\,\mathrm{A\,m^{-2}}$ and $J_{\mathrm{dep}} = 12.75 \times 10^{10}\,\mathrm{A\,m^{-2}}$, with the latter corresponding to a maximum current intensity of $7.6\,\mu$A in the nanowire. The working window of such a device has the desirable quality of lying in a low-current density range, which allows us to avoid Joule heating effects and significant temperature gradients in proximity of the constriction[40].

Spin Wave Emission. Upon the application of a current $J_{\mathrm{rot}} < J_c < J_{\mathrm{dep}}$ through the wire, the domain wall is driven towards the right and, after a transient time of a few ns (see Fig. 1b), reaches a stationary position below the notch, where it slightly oscillates back and forth (see Fig. 1b) while its spins rotate clockwise in the strip plane, as shown in Fig. 1c and in movie A of the supplementary material. Because of the reduced lateral dimension of the wire, DW rotation is coherent and its spins rotate synchronously. Examining the normalized x- component of magnetization $m_x = M_x/M_s$, as shown in Fig. 2a and in movie A in the supplementary material for $J_c = 6.5 \times 10^{10}\,\mathrm{A\,m^{-2}}$, we observe the presence of the characteristic pattern of SWs propagating to the right side of the strip, whereas a much weaker propagation is observed on the left side. In Fig. 3a we monitored the value of the x- component of magnetization averaged over the whole strip, $\langle m_x \rangle$ (dark blue line) and observed its value oscillate around zero at the frequency $f_{DW} = 6.6$ GHz. If we examine the average over a $1.35\,\mu$m long region R, located 400 nm from the DW (light green line), we observe a smaller oscillation at higher frequency. By taking the Fourier transform of these two signals (Fig. 3b), we observe a peak at $f_{DW} = 6.6$ GHz, while the main signal from the region R represents the SW frequency $f_{SW} = 33$ GHz. The secondary peak in the global signal, corresponding to $3f_{DW}$, represents an odd higher harmonic. To gain more insight into the magnetization dynamics, we examine the frequency signal distribution over space (Fig. 3c) by taking the Fourier transform of $m_x(t, \mathbf{r})$ at every cell situated along the x- central axis of the strip. A large amplitude can be observed at the centre of the strip where the DW rotates, remaining pinned below the notch, with the largest amplitude at the frequency f_{DW}, at which the DW rotates fully in-plane. Additional peaks at odd multiples of f_{DW} can be seen with a propagating branch corresponding to the fifth harmonic, indicating a definite propagation of the SW towards the right. Taking the Fourier transform in space and time of $m_x(t, \mathbf{r})$ in the same central row of cells restricted to region R, we obtain the $f-k$ diagram showing a single focused spot corresponding to f_{sw} (Fig. 3-d). The analytical dispersion relation for exchange spin waves in our sample is also shown in the figure:

$$\omega(\mathbf{k}) = \omega_0 + \omega_M \lambda_{\mathrm{ex}}^2 \mathbf{k}^2, \tag{2}$$
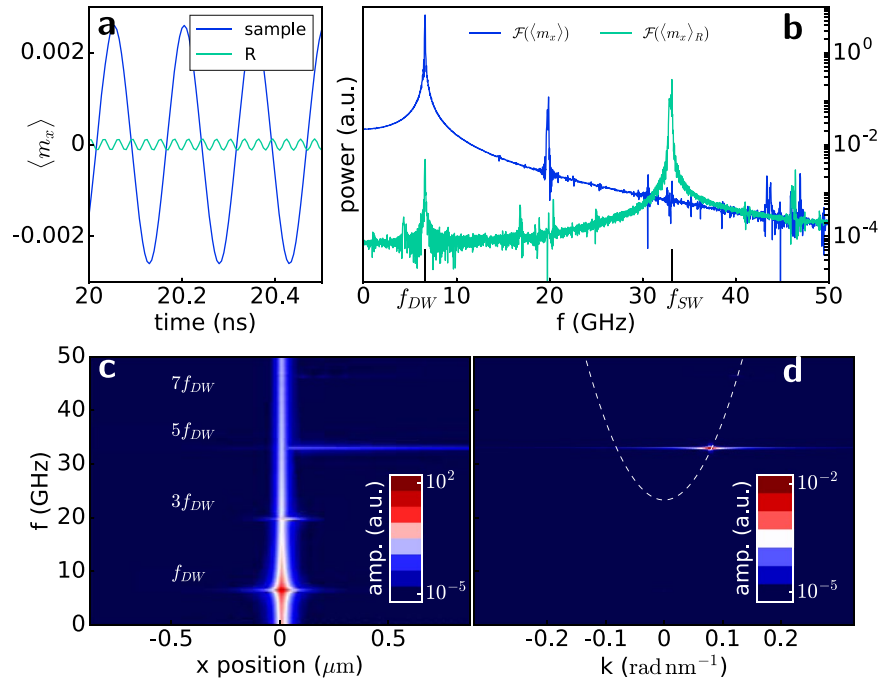
3

Figure 3. Study of DW rotation frequency and SW emission frequency. (**a**) Evolution of the averaged $x-$component of the normalized magnetization during a time window of $0.5\,$ns. The dark blue line shows averaging over the whole sample and the light blue line shows the averaging over the region R away from the DW. Different periodicities can be observed. (**b**) Fourier transform of the time signals shown in (**a**) the dark blue line shows the main peak at the frequency of rotation of the DW f_{DW}, and the light blue line has the principal peak at the SW propagation frequency $f_{SW} = 5f_{DW}$. (**c**) Frequency spectrum of $m_x(t)$ as a function of $x-$ position at the center of the strip width. Peaks centred at the DW position with an odd multiple frequency of f_{DW} are marked. (**d**) $f - k$ diagram extracted from the central line in region R shows a focused peak lying over the right principal branch of the analytical dispersion relation, marked as a dashed line.

where $\omega_0 = \gamma_0(H_{k,\text{eff}} + H_a)$, $H_{k,eff}$ is the effective out-of-plane anisotropy, $\omega_M = \gamma_0 M_s$ and $\lambda_{\text{ex}}^2 = \frac{2A}{\mu_0 M_s^2}$. Indeed, $f_{SW} = 5f_{DW} = 33\,$GHz is the first odd harmonic that is allowed to propagate in the system, being above the threshold frequency $f_0 = \omega_0/2\pi = 23.3\,$GHz. This emission of SWs has the remarkable property of being unidirectional, coherent and directly dependent on the applied current density as we will discuss below.

Varying the applied current intensity between J_{rot} and J_{dep} leads to different DW rotation frequencies extracted from $\mathcal{F}(\langle m_x \rangle)$, as shown in Fig. 4a,b. It is predicted by the analytical model[32] that a linear relationship exists between f_{DW} and the applied current. However, the DW rotation position varies with applied current, thus changing the local current density at the DW position; as a result, the DW rotation frequency is not linear with nominal applied current. The linear dependence between the applied current and f_{DW} is recovered if we consider the actual current density flowing at the DW position (see the supplementary information). In addition, the amplitude of the signal increases with current density, as denoted by the size of the hexagons in Fig. 4b. This observation is due to the fact that $\langle m_x \rangle$ oscillation increases with J_c because the DW moves further away from the centre of the notch and, therefore, the number of spins precessing also increases.

If we now examine the frequency spectrum away from the notch, we observe a different distribution of amplitude peaks with J_c. In Fig. 4c, peaks in the frequency signal sampled over region R are plotted against the applied current density with different colours and sizes to mark their amplitude. Dashed blue lines denote the frequency-current density curve of the rotating DW and its odd higher harmonics. As can be observed, all peaks lie on odd harmonics of f_{DW}, and their amplitude is maximum when SW can actually propagate, i.e., above the threshold frequency f_0. The frequency gap region where propagation is forbidden is shaded in blue. The highest emission intensity is achieved for current densities between 4.5 and 7 $\times$ $10^{10}\,$A m^{-2} on the fifth harmonic, which is the first branch largely above the propagation threshold f_0. Emission is highly coherent with linewidths below $150\,$MHz.

Application of external field.

To extend the operating window of the device, we apply an external field opposing the driving force exerted by the STT. In our situation this means applying an external field H_a pointing into the plane along the $-\hat{\mathbf{z}}$ direction. We can estimate such an effect by means of the one-dimensional model: the external field together with the pinning effective field must balance the STT so that we have a linear dependence of the depinning current on the external field:
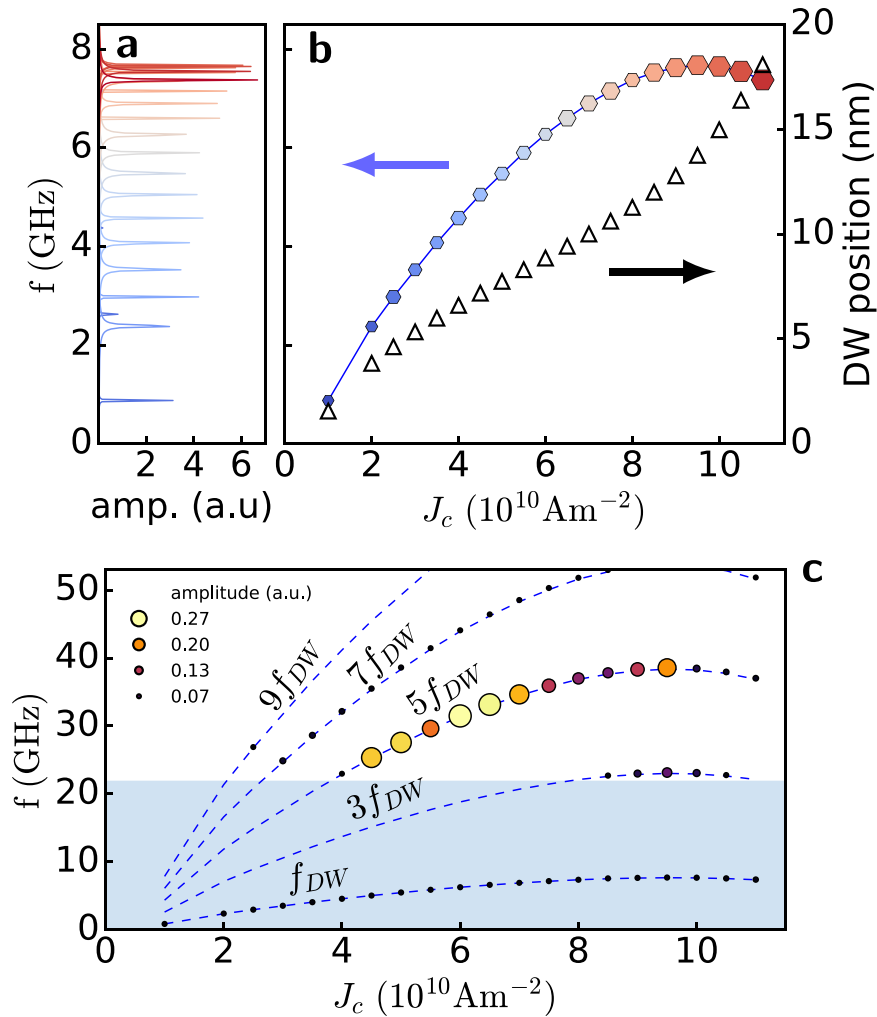
Figure 4. Frequency study of DW rotation and SW emission. (**a**) Frequency spectra of $\langle m_x \rangle$ showing the peaks from which f_{DW} is extracted. (**b**) DW frequency (full hexagons) as a function of applied current extracted from the peaks in (**a**) the size of the hexagons is proportional to the height of the peaks. Average DW position in the pinned rotation regime for the corresponding current (triangles). (**c**) Principal peaks in the frequency spectrum extracted from region R away from the DW. The peak amplitude is denoted by the circle size and the colour scale, (dark to bright). The dashed lines denote f_{DW} as in (**b**) and its odd multiples. The shaded region denotes the non-propagating frequency gap $f < f_0$.

$$J_{\text{dep}}(H_a) = \frac{eM_s}{P\mu_B}\frac{\alpha\gamma_0\Delta}{1 + \alpha\beta}\Big(H_p(\overline{q}) + H_a\Big) = J_{\text{dep}}^0 + \frac{eM_s}{P\mu_B}\frac{\alpha\gamma_0\Delta}{1 + \alpha\beta}H_a,$$

(3)

where J^0_{dep} is the threshold current for depinning without an applied field from equation (1).

The increase in the depinning current in the presence of an external field is shown in Fig. 5a together with the analytical prediction (3) (dashed line). Threshold current J_{dep} increases almost linearly with the applied field for a wide range of fields, with 120 mT giving a 100% increment of the depinning current at zero field. In this manner, we can extend the current density window for DW rotation and achieve f_{DW} up to 15.7 GHz as shown in Fig. 5c. An interesting consequence of the application of an into-the-plane field is its antisymmetric contribution to the effective field in the two magnetic domains in which our strip is divided, which leads to the vertical displacement of the left and right propagating branches (Fig. 5b), depending on the relative orientation with the magnetization.

This splitting of the dispersion relation in the left and right domains opens the possibility of SW propagation in the left domain. In fact, for an applied field of 300 mT, $f(k = 0) = f_0 = 23.3$ GHz becomes $f_0^R = 31.4$ GHz and $f_0^L = 14.6$ GHz for the right and left domains, respectively, with the latter being below f_{DW} for a wide range of J_c (see Fig. 5c,d). We perform simulations with an external applied field $-H_a\hat{z}$ with $\mu_0 H_a = 300$ mT and we monitor the magnetization in two regions L and R, both of them 2 μm long and situated 1.296 μm from the centre of the strip, as shown in Fig. 2b. The DW rotation frequency is extracted as usual as $\mathcal{F}(\langle m_x \rangle)$ and is plotted in Fig. 5c. In Fig. 5d, the peaks in frequency of $m_x(t)$ in the two sampled regions are plotted, where the size of each
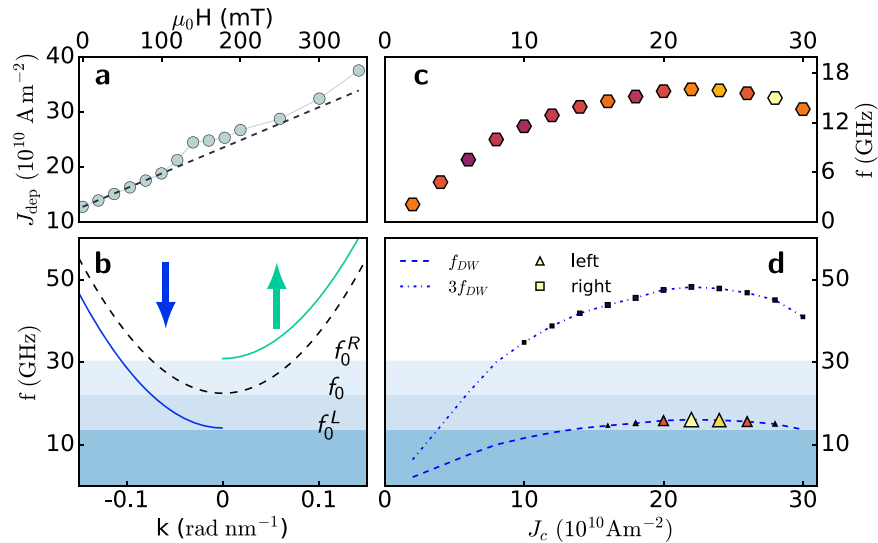
Figure 5. DW rotation and SW dynamics in the presence of an external field. (**a**) Depinning current J_{dep} as a function of a counter-acting external field applied along the $-\hat{z}$ direction. The dashed line represents the theoretical prediction made using the one-dimensional model (3). (**b**) Splitting of the dispersion relation branches in the positive and negative directions with respect to the DW caused by the application of an external field, as prescribed by equation (2). (**c**) DW rotation frequency as a function of the applied current when an external field of 300 mT is applied. (**d**) SW propagation observed in the regions distant from the DW on the left (triangles) and on the right (squares), as indicated in Fig. 2b. The size of the symbols express the SW amplitude. The SW propagates to the left at f_{DW}, whereas it propagate to the right at $3f_{DW}$.

symbol represents the peak's amplitude. In the left domain (triangles), we have SW propagation towards the left at the DW rotation frequency when this exceeds the propagation threshold frequency f_0^L, and no higher harmonic excitation is observed. On the right side, the third harmonic is now accessible for SW propagation via the increased DW rotation frequency and is the one at which SWs propagate. This result adds an important feature to this spin wave emitter because spin wave propagation can be tuned in two different aspects: the propagation frequency can be regulated by changing the applied current, while bidirectional or unidirectional emission from the DW and additional frequency regulation can be obtained via the application of an external field.

Discussion

This novel scheme for tuneable and short-wavelength SW emission suggests new directions in low-power magnonic devices. Unidirectional and asymmetric spin wave propagation is a peculiar feature of this system. The intrinsically asymmetric character of the Dzyaloshinskii-Moriya interaction (DMI) has been exploited to obtain unidirectional propagation of SWs along nanowires[41] and focusing of SWs in thin films[42]. However, in our system, the effect of DMI is negligible, and the origin of such an effect is purely geometric, as will be shown below. The precession of the domain wall's spins is the source of spin wave excitation, and SW propagation at odd higher harmonic of the DW rotation frequency is the signature of a periodic and non-linear excitation[30,43]. If the simple oscillation of the DW below the notch or its change in width when passing from Néel to Bloch configuration were the main mechanism of excitation, we would observe emission at $2f_{DW}$ and its harmonics. However, the absence in the frequency spectrum of the amplitude peaks at even multiples of f_{DW} makes us disregard this hypothesis.

To shed more light on the excitation mechanism, we focus our attention on the role played by the stray field of the rotating DW. Because of the reduced width of the strip, precession of the spins in the DW occurs in a very coherent fashion, making the DW appear as a dipole rotating in the strip plane, as represented schematically in Fig. 6a. The stray field generated by such a dipole has a strong in-plane component, and it rotates at $f = f_{DW}$. To verify that the DW behaves as a rotating dipole and can be regarded as the main mechanism that excites propagating SWs, we proceed in two steps. First, we examine the SW emission induced in a uniformly magnetized thin film via the external field generated by a point dipole $\mathbf{B}(\mathbf{r}) = \frac{\mu_0}{4\pi}\left(\frac{3\mathbf{r}(\mathbf{m}\cdot\mathbf{r})}{r^5} - \frac{\mathbf{m}}{r^3}\right)$ rotating in-plane at $f = 5\,$GHz.

After a period of transient turbulent dynamics with incoherent emission of SWs, when a stationary regime is reached, we observe an isotropic and rather weak emission of spin waves in all directions (Fig. 6b and movie B of the supplementary information). When 2-dimensional Fourier transform is performed on $m_x(t)$ along a 1.25 μm long line starting 400 nm from the centre of the square, we see in the $f{-}k$ diagram a spot at 5 GHz and $k = 0$ corresponding to the non-propagating oscillation induced directly by the external dipolar field. The principal branch of the propagating SW is also marked, showing a peak at 25 GHz; i.e., emission is stronger at a frequency 5 times larger than the driving rotation rate. In other words, the rotating dipolar field is responsible for excitation of SWs at odd harmonics and such excitation is weak, comparable to the one also observed in the left domain in Fig. 2a. In order to highlight the analogy with the case of the rotating DW, we carve a very deep symmetric notch in the square film to obtain a 20-nm channel in the middle as in the nano wires under examination. We then set an
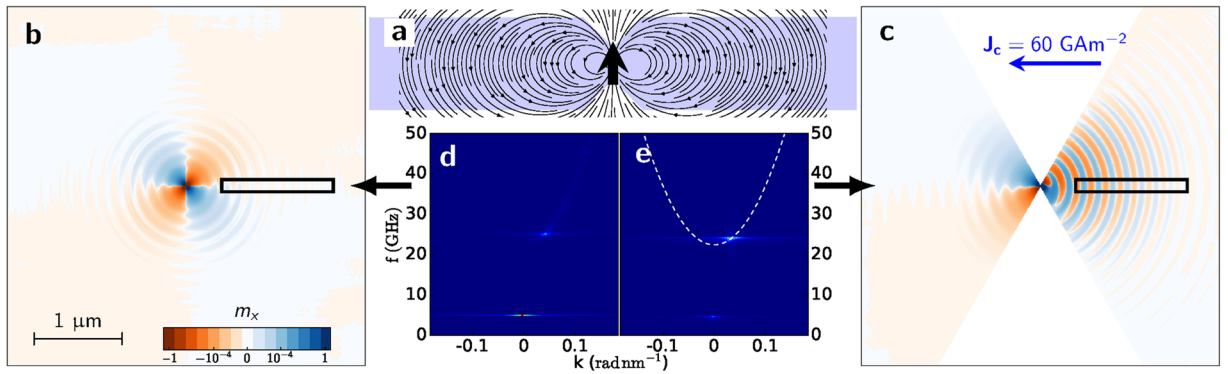
Figure 6. Comparison of the SW excitation caused by a rotating dipolar field and a pinned rotating DW. (**a**) Schematic spatial configuration of the in-plane stray field generated by the DW. (**b**) Snapshot of the magnetization dynamics in a thin film where the excitation is produced by a dipolar field located at the film centre rotating at 5 GHz. (**c**) Snapshot from simulations, where an applied current induces rotation of a DW pinned at the centre. (**d**) $f - k$ diagram extracted from the region indicated in (**b**), showing the non-propagating oscillation at 5 GHz and the propagating one at 25 GHz. (**e**) $f - k$ diagram showing propagation of SWs in the region indicated by the rectangle in (**c**).

up-down magnetization configuration with the DW pinned at the channel and apply a current of $6\,\mathrm{GA\,m^{-2}}$ (uniform for simplicity) that yields a DW rotation frequency $f_{DW} \sim 4.8\,\mathrm{GHz}$. In Fig. 6c, a snapshot representing m_x during the stationary dynamics shows a strong SW emission to the right, whereas the perturbation in the left domain is much weaker and is not capable of exciting SWs, as can also be observed in movie B from the supplementary material. Extracting the $f - k$ diagram from the same spatial region and over the same time span as in the rotating dipole case (Fig. 6e), we find a spot at f_{DW} and $k = 0$, while the spot on the dispersion relation branch is exactly at $24\,\mathrm{GHz} = 5f_{DW}$ with no additional SW emission along the branch.

To further prove the essential role of the DW's stray field in exciting SWs, we run micromagnetic simulations without considering the long-range dipolar interaction; i.e., considering an anisotropy parameter $k_{\mathrm{eff}} = k_u - \frac{1}{2}\mu_0 M_s^2$ that includes the local demagnetizing effect of the dipolar field, we can achieve DW pinned rotation with a behaviour and a rotation frequency very similar to those observed in full simulations (Fig. 7a). However, only a weak dissipative radiation of exchange SWs is present[26,29], and no coherent SW emission at a well defined frequency is observed, as shown in Fig. 7b, where the frequency spectrum at $J_c = 6.5 \times 10^{10}\,\mathrm{A\,m^{-2}}$ is compared with the standard simulations that take into account dipolar interaction. From these observations, we can conclude that the dipolar field of the DW is responsible for the coherent excitation of SWs, behaving as a rotating antenna. However, additional contributions from the wire edges must be considered to explain the unidirectionality. When neglecting dipolar interaction, the DW rotation excites circular oscillations in the spins close to the DW only via exchange interaction passing from Bloch to Néel configuration at f_{DW} frequency. Such perturbation is very strong close to the DW and decays exponentially with distance. On the other hand the magnitude of the DW dipolar field decays as $|\mathbf{r}|^{-3}$ from the DW. In Fig. 8a,b, the magnitude $H = \sqrt{H_x^2 + H_y^2}$ of the in-plane component of both exchange H_{ex}^{ip} and dipolar H_d^{ip} fields is shown in dark to bright colour scale before applying the external current, when the DW is pinned at the centre of the notch pointing upwards and no propagating SW perturbs the configuration. Moreover, when the DW is set into rotation by the application of a current, the in-plane component of the two fields rotates in opposite directions: clockwise H_{ex}^{ip} following the DW rotation and anticlockwise H_d^{ip}, so there is a competition between the excitation of the spins due to the exchange interaction close to the DW and that due to dipolar interaction further away from the DW. Their combined effect results in a strongly elliptical excitation of the magnetization in the region where the two fields have a similar magnitude, as shown in Fig. 8c.

At the wire edges, where in-plane tilt of the spins produces surface charges and an additional stray field component, this effect is strengthened. The fact that the DW is pushed by the STT from the centre of the notch towards the right makes the excitations at the edges much weaker on the left side, where both fields have small in-plane components so that their combined action is not capable of exciting higher harmonics. To prove this point, simulations with a different DW pinning strategy have been performed. A 20% lower uniaxial anisotropy constant k_u in a 30-nm wide band at the centre of the nanowire (indicated by the blue rectangle in Fig. 9a) creates an energetically favourable position for the DW, giving rise to a strong and localized potential well for the DW without changing the local geometry. Applying a current $J_c = 9 \times 10^{10}\,\mathrm{A\,m^{-2}}$ produces SW emission in both directions (as shown in Fig. 9a). This result also proves that the small non-adiabatic torque we use does not play a role in suppressing spin waves that propagate against electron flow, as it has been argued in the literature[44]. Therefore, we conclude that the dipolar field of the rotating DW is responsible for the higher harmonic SW emission, and because this excitation has a dipolar and thus geometrical origin, the displacement of the DW on the right side of the pinning site causes the screening of the emission towards the left side. Such emission is recovered when $f_{DW} > f_0$, and the simple DW rotation can excite the SW towards the left (see Figs 2b and 6d).
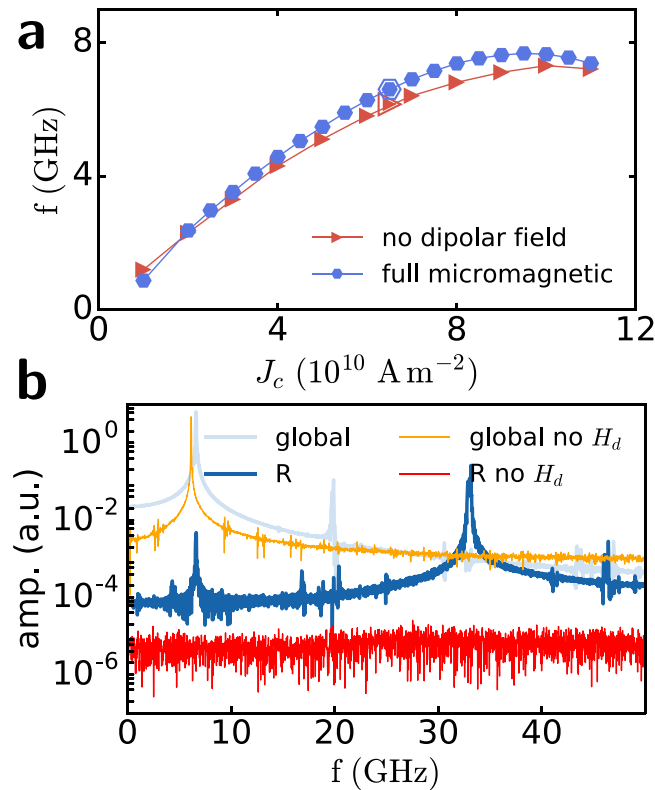
Figure 7. Role of non-local stray field in exciting SWs. (**a**) DW rotation frequency as a function of current for full micromagnetic simulations (blue hexagons) compared with simulations without the non-local effect of the magnetostatic field (orange triangles). (**b**) Fourier transform of $m_x(t)$ averaged over the whole sample and in the region R 400 nm from the notch, as in Fig. 2a (light and dark blue lines), under the application of $6.5 \times 10^{10}\,\mathrm{A\,m^{-2}}$. Simulations without computation of the dipolar fields (orange and red lines) show a single peak at the DW frequency and no signal away from the DW.
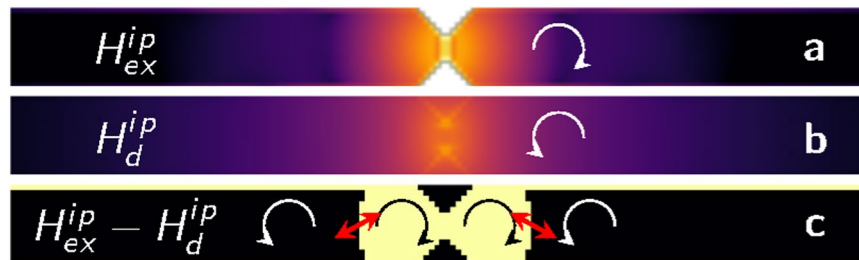

Figure 8. Competition between the in-plane components of exchange and dipolar field is the origin of SW excitation. The intensity of the in-plane component of the exchange field (**a**) and the dipolar field (**b**) for a DW placed at the center of the wire at rest is plotted in dark to bright colour scale. The arrow indicates the direction of rotation of the in-plane component of the field when the DW is led to rotation via an applied current. **c** The sign of $H_{ex}^{ip} - H_d^{ip}$ marked as bright (dark) for positive (negative). Arrows indicate the direction of rotation of the combined in-plane excitation.

In conclusion, we have presented a novel paradigm to excite spin waves via the spin transfer torque-induced rotation of a domain wall pinned at a geometrical constriction in a narrow wire. We showed that by selecting the notch shape and the wire cross section, spin wave emission in the direction of electrons' flow can be achieved for extremely low current densities. Spin wave emission occurs at an odd multiple of the DW rotation frequency up to 40 GHz, without any external applied field. Such spin wave emission is very coherent and of short wavelength down to 60 nm, typical of exchange spin waves. The application of an external field opposing the STT has the twofold effect of extending the operation window of the DW pinned rotation regime on the one hand, achieving higher DW rotation frequencies, and affecting anti-symmetrically the dispersion relation in the two domains on the other hand, thus modulating the SW emission in the direction of electrons flow and allowing propagation in the opposite direction. In other words, the SW emitter can work as unidirectional or asymmetric bidirectional
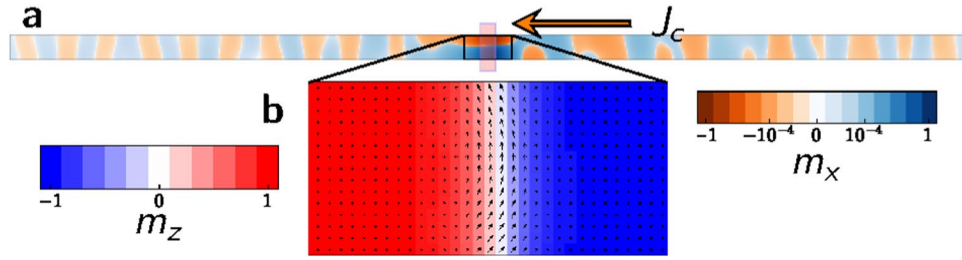
Figure 9. Non-geometrical constriction produces bidirectional SW emission. (**a**) Snapshot of the magnetization dynamics showing the $x-$ component of the magnetization when a DW is forced to rotate via the application of a current density $J_c = 9 \times 10^{10}\,\mathrm{A\,m}^{-2}$. The pinning is realized via a decrease of 20% in uniaxial anisotropy constant k_u in the shaded region. (**b**) Close view of DW mangetization distribution. The DW stretches across the whole wire width and its rotation is no longer uniform, causing a more irregular SW excitation and waveform.

SW emitter depending on the application of an adequate external field. The dipolar field of the rotating DW is the main cause of periodic non-linear excitation of SWs that propagate at higher harmonics of the DW rotation frequency in the system. The displacement of the DW on one side of the notch enhances the excitation on one side and weakens it on the other, giving rise to the unidirectionality.

Methods

Micromagnetic modelling. In our study, we integrate numerically, using a custom finite difference solver, the Landau-Lifschitz-Gilbert (LLG) equation of the magnetization dynamics that includes the contribution of the spin transfer torque caused by the flowing of an in-plane charge current density $\mathbf{J}_c$[22] with spin polarization P and degree of non-adiabaticity β:

$$\frac{d\mathbf{m}}{dt} = -\gamma_0 \mathbf{m} \times \mathbf{H}_{\mathrm{eff}} + \alpha \mathbf{m} \times \frac{d\mathbf{m}}{dt} - (\mathbf{u} \cdot \nabla)\mathbf{m} + \beta \mathbf{m} \times [(\mathbf{u} \cdot \nabla)\mathbf{m}], \qquad (4)$$

Here, e is the negative electron charge, μ_β is the Bohr magneton, $\gamma_0 = 2.21 \times 10^5\,\mathrm{rad\,m\,A^{-1}s^{-1}}$ is the gyromagnetic ratio, α is Gilbert's damping parameter and $\mathbf{u} \stackrel{\mathrm{def}}{=} \mathbf{J}_c \frac{P\mu_B}{eM_s}$.

Material parameters of annealed 1 nm thick $Co_{20}Fe_{60}B_{20}$ as in[45] were chosen: saturation magnetization $M_s = 8.84 \times 10^5\,\mathrm{A\,m}^{-1}$, uniaxial anisotropy constant $k_u = 8.35 \times 10^5\,\mathrm{J\,m}^{-3}$, exchange stiffness $A_{\mathrm{ex}} = 23 \times 10^{-12}\,\mathrm{J\,m}^{-1}$, Gilbert's damping $\alpha = 0.015$. The degree of non-adiabaticity of the spin transfer torque was chosen as $\beta = 2\alpha$ and the polarization coefficient as $P = 0.5$. The CoFeB strip under study is divided into square cells of 4 nm in side and 1 nm thick, with all dimensions below the Bloch length $\sqrt{A/k_u} = 5.25$ nm. To avoid reflection of the SWs and simulate propagation in a much longer nanowire, absorbing boundary conditions are applied at the wire ends in the form of a smoothly augmented damping profile[46]. The spatial configuration of current density $\mathbf{J}_c$ is computed numerically by integrating Laplace's equation. The LLG equation was integrated using a Runge-Kutta, Dormand-Prince predictor-corrector algorithm[47] with embedded error control. Starting with a pinned Bloch DW configuration, simulations were run for 15 ns without saving output to skip the initial turbulent dynamics. Afterwards, simulations were run for 40 ns. The output was written every 5 ps.

One dimensional model for pinned DW rotation. Domain wall dynamics in nanowires is well described by the so-called one-dimensional analytical model[37,38] with the inclusion of the STT[22,39,48]. In its simplest form, the model takes into account the DW position q and the in-plane orientation ϕ of the DW spins. We make use of this model to derive the conditions that must be fulfilled to achieve DW pinned rotation. The two differential equations describing the dynamics of a DW moving along a wire with a geometrical constriction are[33,34]

$$\dot{q} = \frac{\gamma_0 \Delta}{1+\alpha^2}\left[\alpha(H_p(q) + H_a) + \frac{H_K}{2}\sin 2\phi\right] + \frac{1+\alpha\beta}{1+\alpha^2}u, \qquad (5)$$

$$\dot{\phi} = \frac{\gamma_0}{1+\alpha^2}\left[H_p(q) + H_a - \alpha\frac{H_K}{2}\sin 2\phi\right] + \frac{\beta-\alpha}{1+\alpha^2}\frac{u}{\Delta}, \qquad (6)$$

where $H_K = 2K_\perp/\mu_0 M_s$ is the in-plane shape anisotropy field on the DW, Δ is the DW width parameter, $u = |\mathbf{u}|$, H_a is an external field applied along $\hat{\mathbf{z}}$ and $H_p(q) = -(2\mu_0 M_s L_y L_z)^{-1}\frac{\partial V_p(q)}{\partial q}$ represents the pinning field caused by a geometrical constriction at position $q = 0$. We approximate the effect of the geometrical constriction as a parabolic potential well centred at the notch ($q = 0$) with stiffness $k\,(\mathrm{J\,m}^{-2})$ and width ℓ

$$V_p(q) = \begin{cases} \dfrac{k}{2}q^2 & \text{if } |q| < \ell \\ 0 & \text{else} \end{cases}.$$

Data availability.   Data from micromagnetic simulations are available upon request from the corresponding author.

Code availability.   Micromagnetic custom code developed at Universidad de Salamanca can be made available from the corresponding author upon reasonable request.

References

1. Stancil, D. D. & Prabhakar, A. *Spin Waves* (Springer US, Boston, MA, 2009).
2. Kruglyak, V. V., Demokritov, S. O. & Grundler, D. Magnonics. *Journal of Physics D: Applied Physics* **43**, 264001 (2010).
3. Chumak, A. V., Vasyuchka, V. I., Serga, A. a. & Hillebrands, B. Magnon spintronics. *Nature Physics* **11**, 453–461 (2015).
4. Stamps, R. L. *et al*. The 2014 Magnetism Roadmap. *Journal of Physics D: Applied Physics* **47**, 333001 (2014).
5. Chumak, A. V., Serga, A. A. & Hillebrands, B. Magnon transistor for all-magnon data processing. *Nature Communications* **5**, 4700 (2014).
6. Vogt, K. *et al*. Realization of a spin-wave multiplexer. *Nature Communications* **5**, 1–5 (2014).
7. Khitun, A., Bao, M. & Wang, K. L. Magnonic logic circuits. *Journal of Physics D: Applied Physics* **43**, 264005 (2010).
8. Schneider, T. *et al*. Realization of spin-wave logic gates. *Applied Physics Letters* **92** (2008).
9. Klingler, S. *et al*. Spin-wave logic devices based on isotropic forward volume magnetostatic waves. *Applied Physics Letters* **106** (2015).
10. Chumak, A. V. *et al*. Direct detection of magnon spin transport by the inverse spin Hall effect. *Applied Physics Letters* **100**, 1–4 (2012).
11. Mushenok, F. B. *et al*. Broadband conversion of microwaves into propagating spin waves in patterned magnetic structures. *Applied Physics Letters* **111**, 042404 (2017).
12. Whitehead, N. J., Horsley, S. A. R., Philbin, T. G., Kuchko, A. N. & Kruglyak, V. V. Theory of linear spin wave emission from a Bloch domain wall. *Physical Review B* **96**, 064415 (2017).
13. Demidov, V. E., Urazhdin, S. & Demokritov, S. O. Direct observation and mapping of spin waves emitted by spin-torque nano-oscillators. *Nature materials* **9**, 984–988 (2010).
14. Madami, M. *et al*. Direct observation of a propagating spin wave induced by spin-transfer torque. *Nat Nanotechnol* **6**, 635–638 (2011).
15. Demidov, V. E. *et al*. Magnetic nano-oscillator driven by pure spin current. *Nature Materials* **11**, 1028–1031 (2012).
16. Kajiwara, Y. *et al*. Transmission of electrical signals by spin-wave interconversion in a magnetic insulator. *Nature* **464**, 262–266 (2010).
17. Rovillain, P. *et al*. Electric-field control of spin waves at room temperature in multiferroic BiFeO3. *Nature Materials* **9**, 975–979 (2010).
18. Weiler, M. *et al*. Elastically driven ferromagnetic resonance in nickel thin films. *Physical Review Letters* **106**, 1–4 (2011).
19. Cherepov, S. *et al*. Electric-field-induced spin wave generation using multiferroic magnetoelectric cells. *Applied Physics Letters* **104** (2014).
20. Berger, L. Possible existence of a Josephson effect in ferromagnets. *Physical Review B* **33**, 1572–1578 (1986).
21. Slonczewski, J. Current-driven excitation of magnetic multilayers. *Journal of Magnetism and Magnetic Materials* **159**, L1–L7 (1996).
22. Zhang, S. & Li, Z. Roles of nonequilibrium conduction electrons on the magnetization dynamics of ferromagnets. *Physical Review Letters* **93**, 1–4 (2004).
23. Liu, R. H., Lim, W. L. & Urazhdin, S. Spectral characteristics of the microwave emission by the spin hall nano-oscillator. *Physical Review Letters* **110**, 1–5 (2013).
24. Hamadeh, A. *et al*. Full control of the spin-wave damping in a magnetic insulator using spin-orbit torque. *Physical Review Letters* **113**, 1–5 (2014).
25. Awad, A. A. *et al*. Long-range mutual synchronization of spin Hall nano-oscillators. *Nature Physics* **1**, 1–4 (2016).
26. Bouzidi, D. & Suhl, H. Motion of a Bloch domain wall. *Physical Review Letters* **65**, 2587–2590 (1990).
27. Wieser, R., Vedmedenko, E. Y. & Wiesendanger, R. Domain wall motion damped by the emission of spin waves. *Physical Review B* **81**, 024405 (2010).
28. Wang, X. S., Yan, P., Shen, Y. H., Bauer, G. E. W. & Wang, X. R. Domain wall propagation through spin wave emission. *Physical Review Letters* **109**, 1–4 (2012).
29. Le Maho, Y., Kim, J. V. & Tatara, G. Spin-wave contributions to current-induced domain wall dynamics. *Physical Review B - Condensed Matter and Materials Physics* **79** (2009).
30. Xia, H., Chen, J., Zeng, X. & Yan, M. Doppler effect in a solid medium: Spin wave emission by a precessing domain wall drifting in spin current. *Physical Review B - Condensed Matter and Materials Physics* **93**, 1–5 (2016).
31. Van de Wiele, B. & Hämäläinen, S. J. Baláž, P., Montoncello, F. & van Dijken, S. Tunable short-wavelength spin wave excitation from pinned magnetic domain walls. *Scientific Reports* **6**, 21330 (2016).
32. Ono, T. & Nakatani, Y. Magnetic domain wall oscillator. *Applied Physics Express* **1**, 0613011–0613013 (2008).
33. Bisig, A., Heyne, L., Boulle, O. & Kläui, M. Tunable steady-state domain wall oscillator with perpendicular magnetic anisotropy. *Applied Physics Letters* **95** (2009).
34. Martinez, E., Torres, L. & Lopez-Diaz, L. Oscillator based on pinned domain walls driven by direct current. *Physical Review B* **83**, 174444 (2011).
35. Ghosh, B. & Solanki, G. Domain wall oscillators. *Applied Physics A: Materials Science and Processing* **118**, 101–106 (2014).
36. Koyama, T. *et al*. Observation of the intrinsic pinning of a magnetic domain wall in a ferromagnetic nanowire. *Nature Materials* **10**, 194–197 (2011).
37. Schryer, N. L. & Walker, L. R. The motion of 180° domain walls in uniform dc magnetic fields. *Journal of Applied Physics* **45**, 5406–5421 (1974).
38. Mougin, A., Cormier, M., Adam, J. P., Metaxas, P. J. & Ferré, J. Domain wall mobility, stability and Walker breakdown in magnetic nanowires. *Europhysics Letters (EPL)* **78**, 57007 (2007).
39. Thiaville, A., Nakatani, Y., Miltat, J. & Suzuki, Y. Micromagnetic understanding of current-driven domain wall motion in patterned nanowires. *Europhysics Letters (EPL)* **990**, 5 (2004).
40. Moretti, S., Raposo, V. & Martinez, E. Influence of Joule heating on current-induced domain wall depinning. *Journal of Applied Physics* **119** (2016).
41. Brächer, T., Boulle, O., Gaudin, G. & Pirro, P. Creation of unidirectional spin-wave emitters by utilizing interfacial Dzyaloshinskii-Moriya interaction. *Physical Review B* **95**, 064429 (2017).
42. Kim, J. V. & Stamps, R. L. & Camley, R. E. Spin Wave Power Flow and Caustics in Ultrathin Ferromagnets with the Dzyaloshinskii-Moriya Interaction. *Physical Review Letters* **117**, 1–5 (2016).
43. Wang, W. *et al*. Magnon-driven domain-wall motion with the Dzyaloshinskii-Moriya interaction. *Physical Review Letters* **114**, 1–5 (2015).
44. Seo, S. M., Lee, K. J., Yang, H. & Ono, T. Current-induced control of spin-wave attenuation. *Physical Review Letters* **102**, 100–103 (2009).

45. Herrera Diez, L. *et al.* Controlling magnetic domain wall motion in the creep regime in He + -irradiated CoFeB/MgO films with perpendicular anisotropy. *Applied Physics Letters* **107**, 032401 (2015).
46. Consolo, G., Lopez-Diaz, L., Torres, L. & Azzerboni, B. Boundary conditions for spin-wave absorption based on different site-dependent damping functions. *IEEE Transactions on Magnetics* **43**, 2974–2976 (2007).
47. Dormand, J. R. & Prince, P. J. A reconsideration of some embedded formulae. *Journal of Computational and Applied Mathematics* **15**, 203–211 (1986).
48. Beach, G. S. D., Tsoi, M. & Erskine, J. L. Current-induced domain wall motion. *Journal of Magnetism and Magnetic Materials* **320**, 1272–1281 (2008).

Acknowledgements

Author Contributions

M.V. performed the simulations, analysed the data and wrote the manuscript. L.L.D. conceived the study and analysed the data. E.M. developed the analytical model interpretation and contributed in explaining the unidirectionality. All authors reviewed the manuscript.

Additional Information

Supplementary information accompanies this paper at https://doi.org/10.1038/s41598-017-13806-1.

Competing Interests: The authors declare that they have no competing interests.

Publisher's note: Springer Nature remains neutral with regard to jurisdictional claims in published maps and institutional affiliations.